



Research article

Towards virtual surgery planning: the modified Blalock-Taussig Shunt

Stephen Haller¹, Rabin Gerrah² and Sandra Rugonyi^{1,*}

¹ Department of Biomedical Engineering, Oregon Health & Science University, 3303 SW Bond Ave., Portland, OR 97239, USA

² Samaritan Cardiovascular Surgery, Stanford University, 3640 NW Samaritan Dr., Suite 100B, Corvallis, OR 973301, USA

* **Correspondence:** Email: rugonyis@ohsu.edu; Tel: +15034189310.

Abstract: A modified Blalock-Taussig shunt (MBTS) is an aortopulmonary shunt to establish or augment pulmonary perfusion in congenital cardiac defects with limited pulmonary blood flow. Proper function of this shunt is of utmost importance. In clinical practice, prediction of flow in an MBTS relies on previous experience. In the research field, computational modeling techniques have been developed to simulate flow in an MBTS and predict its performance. These techniques are promising but also time consuming and prone to uncertainties; therefore not yet suitable for clinical practice. Here we present a simplified, patient-based computational model to predict mean circulatory flow characteristics after MBTS insertion. Simulations performed over a range of pulmonary vascular resistances, were compared to data from: i) previous modeling studies; ii) data from the specific patient modeled, and iii) a cohort of patients with MBTS. Model predictions were within one standard deviation from cohort data; and within 1% from results of previous (more complex) computational models. In comparison to previous studies, our model is computationally stable with significantly shorter computational time to perform simulations. We envision that our approach could be used in the future to perform virtual surgeries, quickly testing different surgical scenarios using the patient own geometrical and physiological characteristics, to aid surgeons in decision making.

Keywords: multiscale computational model; cyanotic congenital heart disease; heart defects; pulmonary atresia; steady state flow

1. Introduction

Cyanotic congenital heart disease (CCHD), or ‘blue baby syndrome’, occurs due to a defect in the heart that prevents separation of oxygenated from deoxygenated blood and/or limits flow to the lungs. As a result, the heart pumps blood that is not fully oxygenated and cannot sustain the demands of the body. Systemic to pulmonary shunt procedures are the mainstay in treatment of congenital heart diseases with limited pulmonary blood flow. The shunt, which in essence is a connecting tube, diverts blood that goes to the body into the lungs, enhancing blood oxygenation. The modified Blalock-Taussig shunt (MBTS; also referred to as modified Blalock-Taussig-Thomas shunt or MBTTS) is the most commonly used shunt for this purpose. Depending on the defect pathology, the shunt constitutes either a sole pulmonary blood provider or an auxiliary pathway that increases pulmonary blood flow to ameliorate oxygenation.

Despite numerous improvements, MBTS overall mortality and composite morbidity rates remain relatively high at 7.2% and 13.1%, respectively [1]. The major causes of morbidity and mortality after MBTS insertion are: 1) MBTS occlusion, which frequently occurs due to coagulation inside the shunt as a result of slow flow conditions; and 2) over-shunting, which basically results in pulmonary over-circulation [2,3]. The key to avoid occlusion and over-shunting complications is to maintain a properly balanced flow of blood: to the lungs, reaching adequate pulmonary perfusion; and through the shunt, minimizing thrombosis risks. Determining the shunt characteristics that are better suited to achieve this goal could be done through virtual surgery approaches: computer simulations that, given shunt characteristics, baby cardiovascular geometries, and physiological conditions, precisely predict outcomes of interventions [4]. In the context of a balanced circulation, the outcome sought is the blood flow dynamics resulting from placement of the shunt. Current virtual surgery approaches, however, present two main limitations: i) prediction accuracy; and ii) time required (and computational resources needed) to perform the simulation [5]. Our study attempts to overcome these limitations.

Simulations of blood flow in the MBTS have progressively become more refined. Flow simulations are now performed using dynamic multiscale models that solve for flow velocities and pressures over several cardiac cycles, using conditions that approximate the patient response from the systemic circulation [6–11]. One of the limitations of this approach is that it requires extensive computational time (on the order of days in a super computing cluster), limiting the number of virtual surgery cases that can be simulated while the patient is waiting for interventions. To overcome this difficulty, in this study we explore the accuracy and efficiency of simply computing average per cycle values of flow variables. As expected, this approach drastically decreases computational time (to a couple of hours at most), while accurately estimating clinically relevant mean flow parameters including cardiac index (CI), the ratio of pulmonary to systemic blood flow (Q_p/Q_s), and systemic oxygen delivery (OD).

To assess the accuracy of simulations, model predictions were compared to clinical data, both patient specific data and previously published data from a cohort of MBTS patients [12]; as well as a previously developed dynamic multiscale computational model [7]. Moreover, we performed simulations in which a patent ductus arteriosus (PDA) was either left intact or resected after MBTS insertion, to determine the impact of a PDA on blood flow dynamics. The PDA is a fetal vessel that allows blood to bypass the non-functional lungs before birth. This conduit, however, closes due to increased blood oxygenation right after birth, but can be kept open in babies with cyanotic heart

defects to improve oxygenation to the lungs (due to pressure differences, after birth blood flow through the PTA in cyanotic babies reverses direction and directs blood from the systemic circulation to the lungs). Herein we describe our proposed approach in details highlighting its advantages, disadvantages, and possible future applications.

2. Materials and methods

2.1. Patient data

Table 1. Patient specific clinical data.

Parameter	Unit	Value
Age	days	16
Sex		F
Weight	kg	3.9
Body surface area (BSA)	m ²	0.25
Heart rate	Beats/min	125
Hemoglobin concentration (Hb)*	d/dL	11.7
Whole body oxygen consumption (CV _{O2})*	mL/(min m ²)	134.4
Pulmonary vascular resistance (PVR _{index})*	mmHg m ² min/L	3.4
Systemic vascular resistance (SVR _{index})*	mmHg m ² min/L	18
MBTS diameter (D _{MBTS})*	mm	3.5
Diameter of patent ductus arteriosus (D _{PDA})* [‡]	mm	4.0
Systemic arterial oxygen saturation (Sat _A)	%	76
Systemic venous oxygen saturation (Sat _{SV})	%	48
Systemic pulmonary venous oxygen saturation (Sat _{PV})	%	95
Pulmonary flow rate (Q _P)	L/min	0.49
Systemic flow rate (Q _S)	L/min	0.71
Cardiac output (CO)	L/min	1.2
Cardiac index (CI)	L/(min m ²)	4.8
Pulmonary arterial pressure (PAP)		
Systolic	mmHg	23
Diastolic	mmHg	21
Mean	mmHg	22
Systemic arterial pressure (SAP)		
Systolic	mmHg	85
Diastolic	mmHg	50
Mean (MAP)*	mmHg	67

Data was collected after MBTS insertion, except patent ductus arteriosus data, which was collected preoperatively ([‡]). General parameters used in model are marked with an asterisk (*). Vascular resistances are given here as an index, which multiplies the resistance value by body surface area (BSA).

We retrospectively obtained patient data from a neonate with a complex CCHD who underwent MBTS insertion as part of palliation. The study was approved by the Oregon Health & Science

University Institutional Review Board (IRB00011857). Patient data (see Table 1), which included a computed tomography angiography (CTA) image, were obtained from postoperative clinical procedures. Systemic vascular resistance (SVR), pulmonary vascular resistance (PVR), mean arterial pressure (MAP), hemoglobin concentration (Hb) and body oxygen consumption (CV_{O_2}) from the patient were used as input variables for our model; while other parameters (CI, Q_p/Q_s , OD, oxygen saturations) were used for model validation and to evaluate model predictions.

2.2. Multiscale model of the MBTS circulation

A multiscale computational model was employed to simulate blood flow through the infant circulation. It consisted of two coupled models: a 3D computational fluid dynamics (CFD) model of blood flow in and around the MBTS; and a lumped parameter network (LPN) model that accounted for the effect of the infant circulation on MBTS blood flow. The integrated model, based on [6], was implemented using a custom MATLAB R2014a (The MathWorks, Inc., Natick, MA) code that interfaced with the CFD solver ADINA-F v9.0.6 (ADINA R&D, Inc., Watertown, MA). The geometry of the 3D CFD model (Figure 1) was derived from the patient CTA image; while the LPN model incorporated patient-specific systemic and pulmonary vascular resistances (SVR and PVR, respectively; Figure 2). The heart was modeled as a constant pressure generator, with aortic blood pressure equal to the patient specific MAP (67 mmHg).

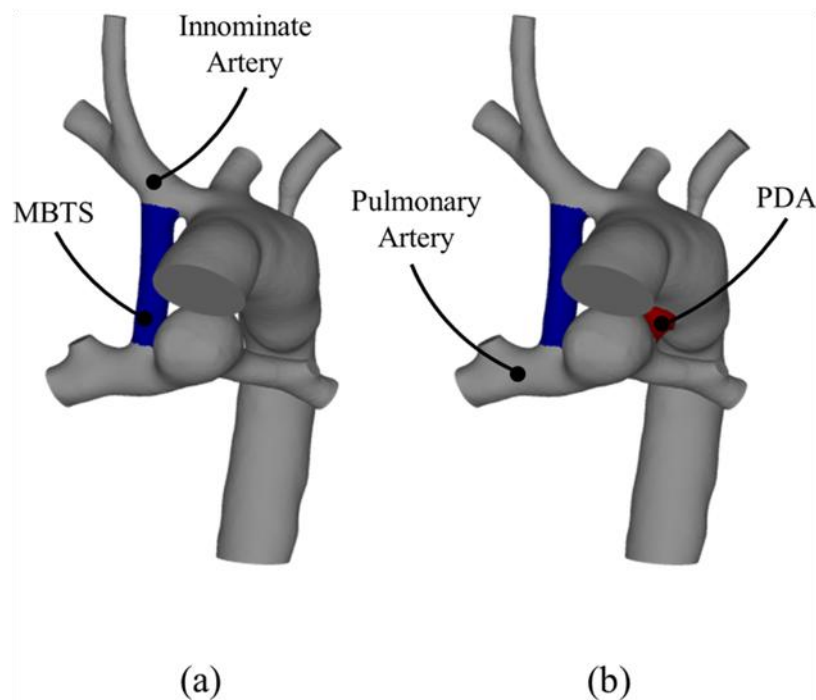


Figure 1. 3D models employed. (a) Patient specific anatomy with a 3.5 mm modified Blalock-Taussig shunt (MBTS) (blue). (b) Artificial anatomy with MBTS and a 4.0 mm patent ductus arteriosus (PDA) (red).

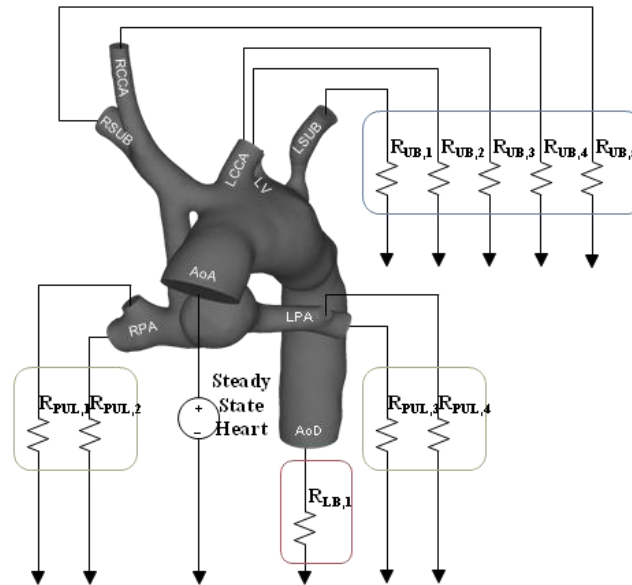


Figure 2. Computational model: 3D model (MBTS anatomy shown) coupled with a lumped parameter network (LPN) model. Blocks correspond to different vascular compartments including: upper body (UB), lower body (LB), and pulmonary (PUL) compartments. The 3D model has one inlet, the ascending aorta (AoA). There are six systemic outlets: right common carotid artery (RCCA), right subclavian artery (RSUB), left common carotid artery (LCCA), left subclavian artery (LSUB), left vertebral artery (LV), and descending aorta (AoD). There are four pulmonary outlets: two branches for the right pulmonary artery (RPA) and two branches for the left pulmonary artery (LPA). The heart was modeled as a constant pressure generator of 67 mmHg.

Coupling between the 3D CFD and LPN models was achieved through an iterative algorithm. At each CFD-LPN interface, blood pressure, calculated by the LPN, was imposed to the 3D CFD model as a uniform traction boundary condition. Conversely, flow, the integration of normal velocity over the 3D outlet surfaces, was imposed as an inlet condition to the corresponding LPN. To ensure convergence to equilibrium, iterations were performed until the change in pressure and flow at all 3D-LPN interfaces was less than 0.1% between successive iterative steps.

2.2.1. 3D CFD model: region of interest

The 3D CFD model comprised a portion of the aortic arch, innominate artery, pulmonary arteries, MBTS, and outlets to the carotid, subclavian and vertebral arteries (Figure 1). Surface meshes were imported into ADINA and the model geometry volume was meshed with flow-condition-based interpolation (FCBI) elements, which are stable for a wide range of flows. Simulations assumed that blood flow was incompressible and Newtonian, with a density (ρ) of 1060 kg/m³ and a dynamic viscosity (μ) of 0.004 Pa s [6]. Thus, neglecting the effects of gravity, the equilibrium equations describing the flow of blood in the 3D CFD model are:

$$\mathbf{v} \cdot \nabla \mathbf{v} = -\nabla p + \mu \nabla^2 \mathbf{v} \quad (1)$$

where \mathbf{v} is the flow velocity vector, ∇ is the gradient operator, and ∇^2 the Laplacian operator.

Two different geometries were generated (see Figure 1): 1) MBTS with no patent ductus arteriosus (PDA); and 2) MBTS with PDA, in which an artificial conduit with the patient specific PDA preoperative diameter (4.0 mm) was inserted during mesh generation. These geometries allowed us to perform simulations to determine whether leaving a PDA could be an advantage.

2.2.2. LPN model: systemic and pulmonary systems

Table 2. LPN parameter values used (see also Figure 2).

Parameter	Unit	Value
Overall:		
SVR_{index}	mmHg m ² min/L	18
PVR_{index}	mmHg m ² min/L	3.4
SVR^*	mmHg sec/mL	4.320
PVR^*	mmHg sec/mL	0.816
Systemic circulation:		
$R_{\text{UB, total}}$	mmHg sec/mL	8.640
$R_{\text{UB, } i}$	mmHg sec/mL	43.20
$R_{\text{LB, total}}$	mmHg sec/mL	8.640
$R_{\text{LB, } i}$	mmHg sec/mL	8.640
Pulmonary circulation:		
$R_{\text{PUL, total}}$	mmHg sec/mL	0.816
$R_{\text{PUL, } i}$	mmHg sec/mL	3.264

*Please note unit change. Also the index version (SVR_{index} and PVR_{index}) is the resistance (SVR or PVR, respectively) multiplied by body surface area (BSA). $BSA = 0.25 \text{ m}^2$ (see Table 1). Subindex i , indicates individual resistance. UB: Upper body; LB: Lower body; PUL: Pulmonary.

A simplified LPN (Figure 2; Table 2), was used to model the connection of the 3D CFD model with the rest of the circulation [6]. Vascular resistance (R) was used to simulate the effect of the systemic and pulmonary circulations. The LPN consisted of two subsystems: 1) the systemic, and 2) the pulmonary circulations. The systemic circulation was divided into the upper body and lower body, each of which was assumed to contribute half the total systemic vascular resistance (SVR). Resistance values were set such that the equivalent resistance across the entire systemic circulation was equal to the patient specific SVR ($4.32 \text{ mmHg}\cdot\text{sec}\cdot\text{mL}^{-1}$; see Table 2), and the equivalent resistance across the entire pulmonary circulation was the patient-specific pulmonary vascular resistance ($PVR = 0.816 \text{ mmHg}\cdot\text{sec}\cdot\text{mL}^{-1}$; Table 2). To couple the 3D model to the LPN model, the following boundary condition equations (at vascular outputs) were employed:

$$Q_i = \int_{A_i} \mathbf{v} \cdot \mathbf{n} \, dA \quad (2)$$

$$P_i = Q_i R_i \quad (3)$$

Where Q_i is the volume flow rate of blood exiting the 3D model at output i , \mathbf{n} is a unit vector normal to the 3D output surface, A_i is the area of the output surface, P_i is the pressure imposed by the LPN model onto the 3D model at output i , and R_i is the resistance associated with the output i .

In quantifications, PVR was varied from 20% to 200% of the patient PVR (range of PVR_{index} : 0.68–6.8 mmHg·m²·L⁻¹·min) to simulate the effects of changing PVR in the circulation.

2.3. Oxygen transport model

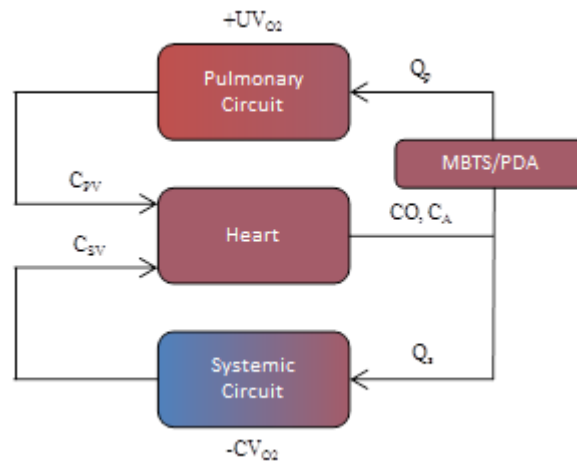


Figure 3. Schematic of oxygen transport model. CO : cardiac output; C_A , C_{SV} and C_{PV} : arterial, systemic venous, and pulmonary venous oxygen concentrations, respectively; Q_s and Q_p : systemic and pulmonary flows, respectively; CV_{O_2} : whole body oxygen consumption; and UV_{O_2} : oxygen uptake by the lungs.

An oxygen transport model, based on [12], was implemented to predict oxygen delivery (OD), systemic arterial saturation (Sat_A), and systemic venous saturation (Sat_{SV}). In the shunted configuration (see Figure 3), oxygen mass conservation establishes:

$$CO \cdot C_A = Q_S \cdot C_{SV} + Q_P \cdot C_{PV} \quad (4)$$

$$CV_{O_2} = Q_S \cdot (C_A - C_{SV}) \quad (5)$$

where, CO is cardiac output ($CO = Q_S + Q_P$), C_A is systemic arterial oxygen concentration, C_{SV} is systemic venous oxygen concentration, C_{PV} is pulmonary venous oxygen concentration, and CV_{O_2} is the patient specific whole body oxygen consumption (134.4 mL min⁻¹ m⁻²; see Table 1).

Pulmonary venous oxygen saturation ($Sat_{PV} = 95\%$; Table 1) was based on patient specific data and pulmonary venous oxygen concentration computed as follows:

$$C_{pV} = O_2 \text{ Cap} \cdot \text{Sat}_{pV} \quad (6)$$

where, $O_2 \text{ Cap}$ is the maximal oxygen carrying capacity (in mL/mL blood, $O_2 \text{ Cap} = 0.0134 \cdot Hb$, where Hb is the patient specific hemoglobin concentration in g/dL). OD was then defined as:

$$OD = C_A \cdot Q_S \quad (7)$$

2.4. Blood flow dynamics and thrombosis

Risk of thrombosis in the MBTS and PDA were estimated based on blood flow dynamics. Like in previous studies, e.g. [7,12], we used the following surrogates associated with thrombotic risk: 1) wall shear stress (WSS), with low values leading to clot formation, and high values to platelet activation leading to coagulation; and 2) residence time (RT), with higher values indicating greater risk of thrombosis due to flow stagnation. We also computed the RT in the pulmonary arteries (PA) as an indicator of over-shunting.

2.4.1. Wall shear stress

WSS were calculated directly from velocity data via post processing in EnSight v10.1.1 (b) (CEI, Inc., Apex, NC) using a custom Python script with the following equations,

$$\boldsymbol{\sigma}(x) = \mu(\nabla \mathbf{v} + (\nabla \mathbf{v})^T) \quad (8)$$

$$\text{WSS}(x) = \|\boldsymbol{\sigma} \mathbf{n} - \mathbf{n}(\mathbf{n}^T \boldsymbol{\sigma} \mathbf{n})\| \quad (9)$$

where, $\boldsymbol{\sigma}(x)$ is the stress tensor evaluated at point x , μ is dynamic viscosity, \mathbf{v} is the velocity vector, \mathbf{n} is the wall surface unit normal vector, ∇ is the gradient operator, and T indicates transposition.

2.4.2. Residence time

RT calculations were performed in EnSight using a particle based method. To measure RT in the MBTS, 1024 evenly spaced particles were ‘emitted’ from a plane intersecting the shunt just below the proximal anastomosis (where flow enters the MBTS). The time for each particle to exit the MBTS, defined as the time it took the particle to reach a plane intersecting just above the distal anastomosis (exiting plane), was recorded. These results were then averaged to calculate mean RT. Similarly, to measure RT in the pulmonary arteries, 1024 particles were emitted from mid-planes intersecting each shunt (i.e. MBTS and PDA) right before flow entered the pulmonary arteries. Particles were then tracked to the boundary of the 3D domain with the time in the 3D modeled portion of the pulmonary arteries recorded.

3. Results

3.1. Mesh sensitivity

To determine the best mesh for simulations, we first completed a mesh convergence analysis. To this end, we performed CFD simulations of the patient 3D geometry, which we progressively meshed with smaller elements. We computed cardiac index (CI) for each simulation, and plotted it versus number of elements in the mesh to determine convergence. CI convergence was defined as the point at which increasing the number of elements in the mesh changed the resulting CI by <1 %. Mesh convergence optimizes computational cost versus accuracy. Convergence was found when average element length was 0.25 mm (~1.5 million elements), and this mesh was then used for all simulations.

3.2. Model results and validation

We simulated the patient-specific model using the selected mesh (~1.5 million elements). An important consideration is that in our model (and the patient simulated) there was no connection between the heart and the pulmonary circulation (the pulmonary artery was blocked in the patient, pulmonary atresia), so that the pulmonary circulation relied on the shunt diverting blood from the systemic circulation. Two cases were considered: 1) the MBTS was the only shunt communicating the systemic and pulmonary circulations; and 2) in addition to the MBTS a PDA was shunting blood to the pulmonary circulation. In addition, we performed simulations in which PVR was changed from 20% to 200% of the patient value, to mimic possible manipulations that surgeons could perform to change PVR in the infant, and determined outcomes. Results obtained are summarized in Table 3.

Table 3. Overall mean circulatory parameter results from our steady state model.

Case	PVR _{index}	CI	Q _p	Q _s	Q _p /Q _s	Sat _A	Sat _{sv}	OD
	mmHg·m ² ·L ⁻¹ ·min		L·min ⁻¹ ·m ⁻²		–	%		mL·min ⁻¹ ·m ⁻²
MBTS								
	0.68	6.87	3.32	3.55	0.94	69.2	45.0	385.2
	3.40	6.65	3.05	3.58	0.85	66.9	42.9	375.6
	6.80	6.35	2.74	3.58	0.77	63.7	39.8	358.4
MBTS w/ PDA								
	0.68	12.00	8.36	3.60	2.32	84.7	61.0	478.8
	3.40	10.48	6.74	3.67	1.84	82.3	58.9	473.6
	6.80	9.08	5.36	3.66	1.46	79.0	55.6	453.2

SVR_{index} = 18 mmHg·m²·L⁻¹·min; Mean P_{AoA} = 67 mmHg; BSA = 0.25 m²

3.2.1. Validation against previous dynamic model

To validate our results (Table 3), we first compared them to cycle-average data from a previously published dynamic model [7]. Comparisons focused on mean flow parameters describing overall circulation performance. We found that flow parameters were extremely consistent between the models, with percent differences for mean CI, Q_p , Q_s and Q_p/Q_s within 1.5% (Table 4). These results suggest our model can accurately capture mean flow characteristics.

Table 4. Comparison of our model results to those from a previous dynamic model study.

Parameter	Unit	Moghadam et al., 2015 (BSA = 0.33 m ²)	Our Model (BSA = 0.25 m ²)	% difference
CI	L·min ⁻¹ ·m ⁻²	8.082	8.164	1.0
Q_s	L·min ⁻¹ ·m ⁻²	4.239	4.300	1.4
Q_p	L·min ⁻¹ ·m ⁻²	3.845	3.864	0.5
Q_p/Q_s	–	0.907	0.899	0.9

SVR = 21.6 mmHg·m²·L⁻¹·min; PVR = 2.3 mmHg·m²·L⁻¹·min; Mean P_{AoA} = 96.8 mmHg; D_{MBTS} = 3.5 mm; % difference = [(steady state – transient)/transient] x 100

3.2.2. Validation against patient data

Predictions from our model were then compared to data from the specific patient modeled as well as clinical data from a cohort of 28 Norwood patients [12], represented as the mean and standard deviation of individual patient data. Clinical data featured only patients who had an MBTS with no PDA. Our model predictions, however, were within one standard deviation of the Norwood cohort averaged data (see Figures 4 and 5). When comparing predicted and patient-specific data, percent differences in CI and Q_p/Q_s were ~40% and ~20%, respectively (Table 5), highlighting uncertainties in both patient-specific measurements and modeling parameters.

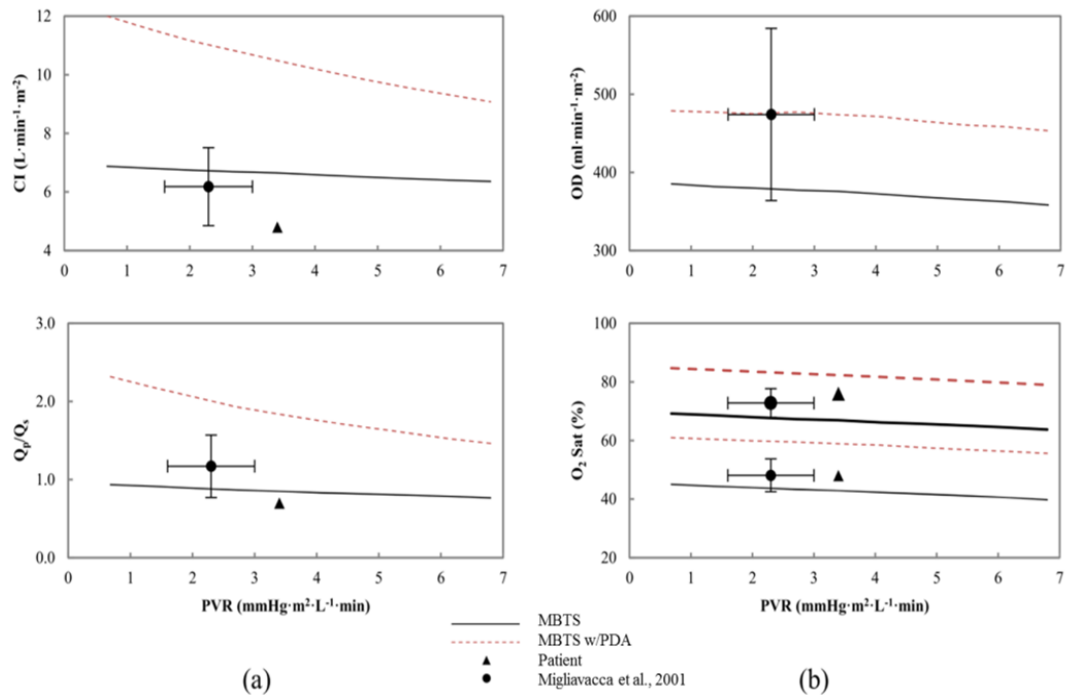


Figure 4. Comparison of mean hemodynamic parameters between model and patient data. (a) Cardiac index (CI) (top) and pulmonary to systemic flow ratio (Q_p/Q_s) (bottom) as functions of pulmonary vascular resistance index (PVR). (b) Oxygen delivery (OD) (top) and oxygen saturation (bottom) as functions of PVR index. For the oxygen saturation graph, thicker lines/markers represent arterial saturation (Sat_A) and thinner lines/markers represent venous saturation (Sat_{SV}). Migliavacca et al., 2001 shows clinical data obtained from 28 Norwood patients [12]; mean \pm SD.

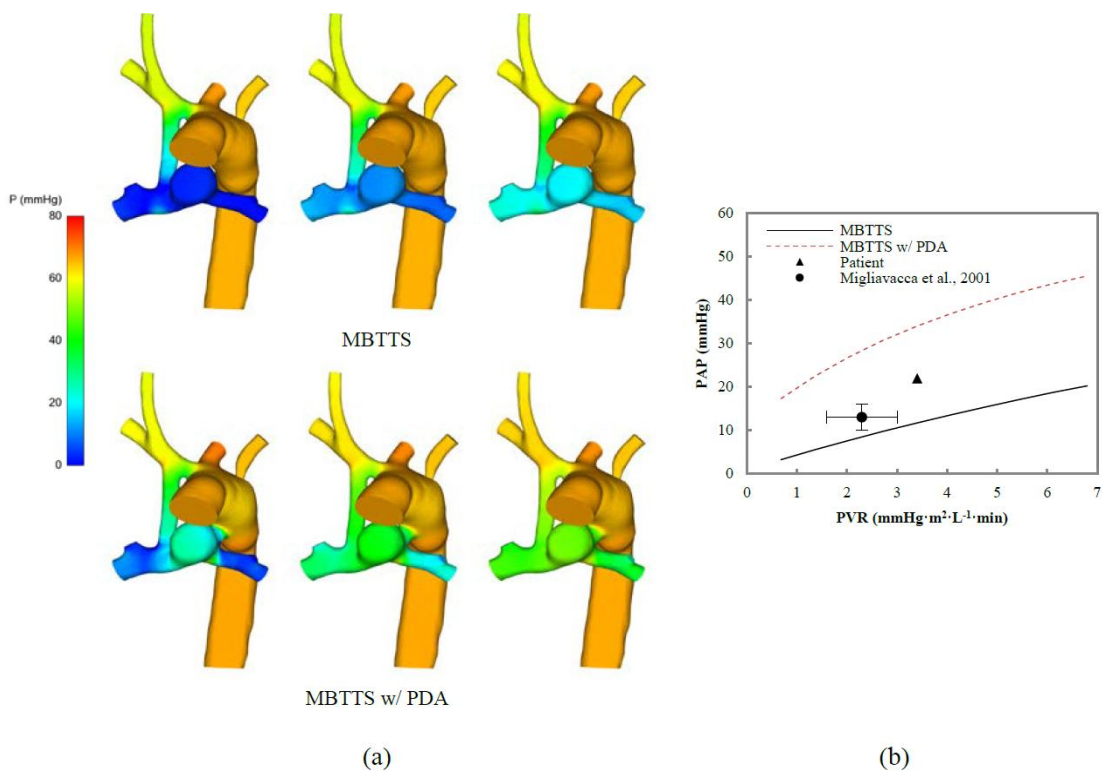


Figure 5. Computed blood pressure drops within the 3D-modeled circulation. (a) Pressure distribution for MBTS (top row) and MBTS w/ PDA (bottom row) at low PVR index (left column; $0.68 \text{ mmHg m}^2 \text{ L}^{-1} \text{ min}$), normal PVR index (center column; $3.4 \text{ mmHg m}^2 \text{ L}^{-1} \text{ min}$), and high PVR index (right column; $6.8 \text{ mmHg m}^2 \text{ L}^{-1} \text{ min}$). (b) Spatially averaged pulmonary artery pressure (PAP) as a function of PVR index.

Table 5. Comparison of our model results to those from the specific patient modeled.

Parameter	Unit	Patient (BSA = 0.25 m^2)	Model (BSA = 0.25 m^2)	% difference
CI	$\text{L} \cdot \text{min}^{-1} \cdot \text{m}^{-2}$	4.80	6.65	38.5
Q_s	$\text{L} \cdot \text{min}^{-1} \cdot \text{m}^{-2}$	2.82	3.58	27.1
Q_p	$\text{L} \cdot \text{min}^{-1} \cdot \text{m}^{-2}$	1.98	3.05	53.9
Q_p/Q_s	–	0.7	0.85	21.5
Sat _A	%	76	75	1.3
Sat _{SV}	%	48	55	14.6

SVR = $18 \text{ mmHg} \cdot \text{m}^2 \cdot \text{L}^{-1} \cdot \text{min}$; PVR = $3.4 \text{ mmHg} \cdot \text{m}^2 \cdot \text{L}^{-1} \cdot \text{min}$; Mean $P_{A_{oA}}$ = 67 mmHg ; D_{MBTS} = 3.5 mm ; % difference = $[(\text{predicted} - \text{observed})/\text{observed}] \times 100$.

3.3. Case results: MBTS alone vs MBTS with PDA

Our results were in general agreement with those of other groups considering similar intervention scenarios with idealized models [6,7,13]. Leaving the PDA intact resulted in a higher CI (increased by 57%) and Q_p/Q_s (increased by 117%) than when considering an MBTS alone (Figure 4a; and Table 3). While Q_s remained relatively constant, Q_p (lung perfusion) increased, leading to higher blood oxygen saturation and increased OD (Figure 4b), at the expense of over-shunting.

Moreover, parameters including CI, Q_p/Q_s , and pulmonary arterial pressure displayed a stronger dependency on PVR when the PDA was intact (e.g. steeper slopes in Figures 4a and 5); with pulmonary arterial pressure (PAP) exhibiting the strongest relationship with PVR. The dependency of blood oxygenation and OD on PVR, however, was relatively weak (Figure 4b).

The presence of a PDA drastically changed local hemodynamics around the MBTS, particularly in the pulmonary arteries (Figure 6). Keeping the PDA decreased flow through the MBTS despite an increase in Q_p . However, the distribution of flow to the right and left pulmonary arteries was slightly more symmetrical when both the MBTS and PDA were present (see Figure 6b).

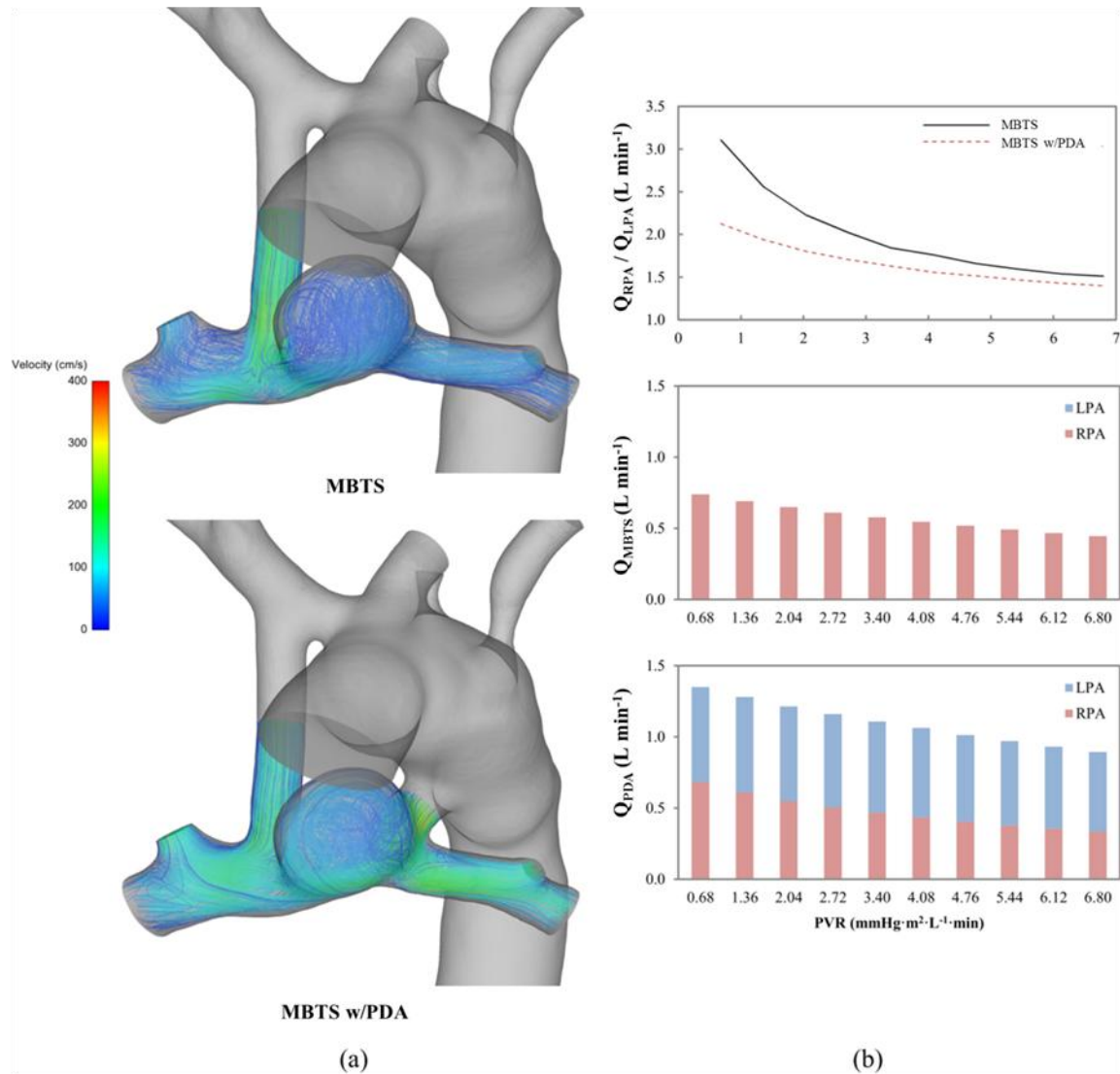


Figure 6. Flow distributions within the 3D-modeled portion of the circulation. (a) Pulmonary artery velocity trace from MBTS (top) and MBTS w/ PDA (bottom) at normal PVR index ($3.4 \text{ mmHg m}^2 \text{ L}^{-1} \text{ min}$). (b) Right pulmonary artery to left pulmonary artery (Q_{RPA}/Q_{LPA}) flow ratio (top), distribution of flow through MBTS in MBTS w/ PDA case to RPA and LPA (middle), and distribution of flow through DA in MBTS w/ PDA case to RPA and LPA (bottom) as functions of PVR index.

3.4. Thrombosis risk and over-shunting indicators

Compared to the case with an MBTS alone, including the PDA increased the spatially averaged WSS over the entire 3D domain by approximately 42% (Figure 7a, b). Because WSS is directly related to velocity, PVR had a greater effect with an intact PDA. On the segment of the pulmonary artery between the MBTS and PDA, where flow competition would be likely to occur, average WSS increased by approximately 116% with the addition of a PDA. Conversely, because flow through the MBTS decreased with PDA, spatially averaged WSS on the MBTS decreased by approximately 25%. The highest WSS ($590 \text{ dyn}\cdot\text{cm}^{-2}$) was observed on the PDA in the case with the lowest PVR. Over

the simulated range of PVR, on average, spatially averaged WSS on the PDA was 32% greater compared to the corresponding MBTS.

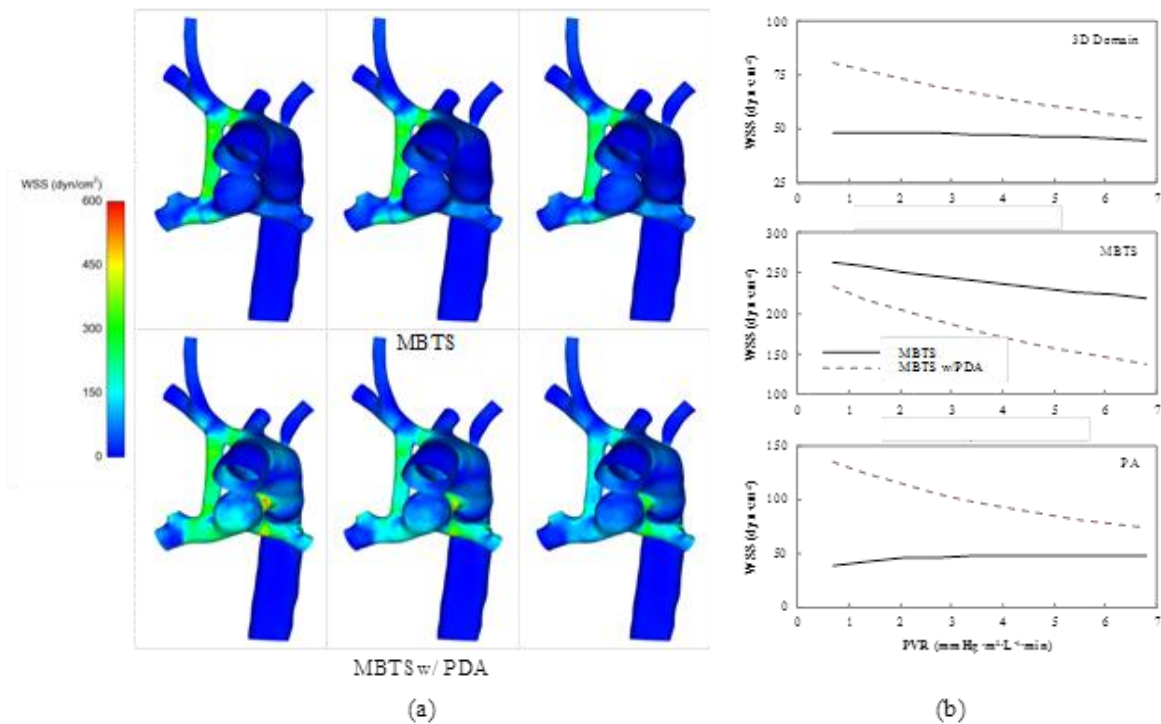


Figure 7. Wall shear stress (WSS) distributions. (a) Wall shear stress (WSS) distribution for MBTS (top row) and MBTS w/ PDA (bottom row) at low PVR index (left column, $0.68 \text{ mmHg m}^2 \text{L}^{-1} \text{min}$), normal PVR index (center column, $3.4 \text{ mmHg m}^2 \text{L}^{-1} \text{min}$), and high PVR index (right column, $6.8 \text{ mmHg m}^2 \text{L}^{-1} \text{min}$). (b) Spatially average WSS over entire 3D domain (top), MBTS (middle), and pulmonary artery (PA) segment between shunts (bottom).

Because PDA caused a decreased flow through the MBTS, mean RT in the MBTS increased by approximately 45% (Figure 8). However, because pulmonary perfusion increased with an intact PDA, RT in the pulmonary arteries decreased by approximately 48% (Figure 8).

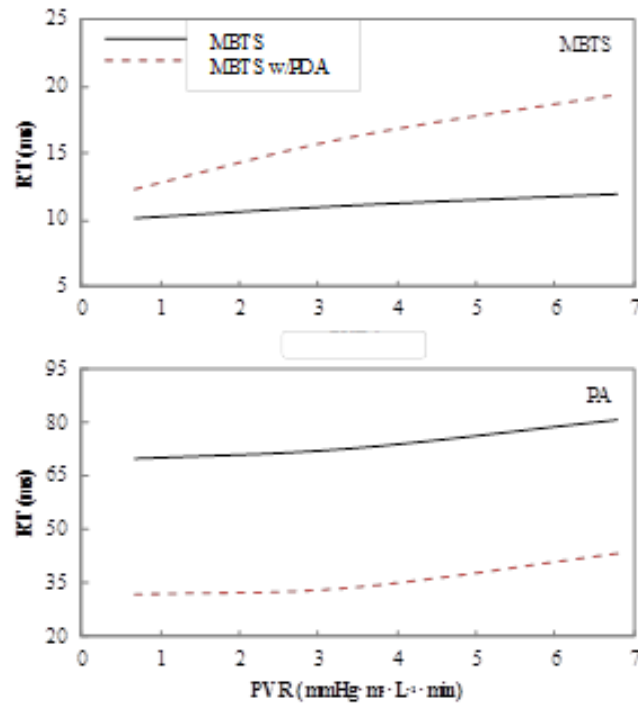


Figure 8. Residence time (RT) of blood. RT in MBTS (top) and pulmonary arteries (PA) (bottom) as a function of pulmonary vascular resistance (PVR) index for both surgical cases.

4. Discussion

As any model, our model of the MBTS circulation has limitations, advantages and disadvantages.

4.1. Model limitations and potential improvements

While physiological flow is pulsatile, our model (by design) does not capture the dynamics of pulsatile flow. Nevertheless, our results compared well with clinical data (e.g. mean flow, CI, Q_p/Q_s), and extremely well with predictions from dynamic models (averaged over the cardiac cycle; Table 4). Therefore our computations allow for a quick screening and testing of different scenarios before selecting the most promising ones for a full dynamic simulation.

The assumption that the heart is a constant pressure source is another limitation. Based on clinical data from a previous study [14], however, during the early postoperative period following MBTS insertion (< 18 hrs), mean arterial pressure (MAP) is about 15% lower in patients with PDA than patients without PDA; but this difference becomes negligible after 18 hrs. Thus, our model describes this later dynamics. In any case, implementation of a simplified cardiac model, while outside the scope of this paper, would circumvent the assumption that the heart is a constant pressure source in the future.

Uncertainties in modeling patient-specific cases remain mainly in finding good mathematical descriptions of the circulation model and properly assessing patient data uncertainties [5,15]. With advances in imaging technologies, uncertainties in delineating and segmenting images for modelling purposes are becoming less of an issue. However, it is still imperative to find accurate parameters for

the LPN models that closely represent the infant circulation under consideration. In this regard, our model used published parameters that were adjusted proportionally only to ensure that SVR and PVR were the same as the patient under consideration. This approach was not enough (see Table 5). While outside the scope of this paper, a thorough uncertainty and sensitivity analysis is required to accurately represent patients and properly manage data uncertainty [15,16]. In particular, resistance values employed are key, and more sensitive than dynamic parameters. Uncertainty and sensitivity analyses will be far easier and effective to perform (at least initially) on our simplified model than in a dynamic model of the infant circulation. To improve our modeling technologies, therefore, future work needs to focus on uncertainty and sensitivity analyses [15].

4.2. *Validity of the approach*

In clinical practice, accurate and meaningful results are needed in the shortest possible time. This is particularly important if time-sensitive intervention decisions were to rely on simulated scenarios. Our approach was designed to compute clinically relevant mean circulation variables (e.g. CI, Q_p/Q_s) at a fraction of the time involved in performing simulations accounting for the dynamics of several cardiac cycles, which can easily take several days to compute even in a supercomputer. Our proposed model (with simulations that take only a few hours) seems sufficient for screening scenarios, from which a few could then be chosen for a more in depth analysis if needed.

Our model results compared well against both a fully dynamic model [7] (Table 4) and patient cohort data [12] (Figures 4 and 5). The small difference between our results and mean data from state-of-the-art dynamic models ($< 1.5\%$) suggests that, in computing mean circulation data, our model performs as well as more involved models. Agreement of our results with cohort data further provides confidence in our model predictive capabilities, although there is room for improvement both in our approach as well as that of others. As mentioned above, we believe that this improvement will require a thorough sensitivity and uncertainty analysis of models.

Differences between patient data and model predictions (Table 4) highlight both measurement errors associated with clinical data and model uncertainties, and were comparable to differences reported when using more involved dynamic models [12]. Future studies addressing these uncertainties are needed to determine the confidence with which we can model a specific patient under consideration, and how this confidence can be improved to increase the accuracy of patient-specific computational predictions [15]. More research is needed in this direction if we are hoping to rely on simulated data for intervention decisions. Our results are beginning to highlight similarities and differences between dynamic and static flow models for evaluating CCHD scenarios and their associated advantages and disadvantages. Simulation of more cases (both dynamic and static) are nevertheless needed to fully develop and validate an effective patient-specific approach.

4.3. *Insights gained*

4.3.1. PVR control

The advantages of noninvasively managing circulation characteristics are inherently obvious. For example, inhaled nitric oxide (iNO) selectively decreases PVR in neonates, including those with pulmonary hypertension [17], providing PVR control. Indeed, model predictions confirm the

effectiveness of managing pulmonary hypertension by decreasing PVR in neonates with an MBTS (Figure 5). With an intact PDA and MBTS the influence of PVR in regulating pulmonary pressure became more pronounced (compared to the case with no PDA; Figure 5). Potential benefits gained from increased PVR response, however, appear to be outweighed by the associated increase in cardiac output and pulmonary perfusion (Figures 4 and 5). Other therapies including sub-atmospheric oxygen and induced respiratory acidosis have been shown to affect PVR as well as other parameters such as SVR [18]. Future studies that model the effects of manipulating multiple variables simultaneously could provide insight into which parameters or combination of parameters result in the most efficient circulatory control techniques.

4.3.2. Thrombosis risk

Previous studies have associated platelet activation and thrombosis with regions of very high and very low WSS [19]. In addition to WSS magnitude, exposure or residence time (i.e. RT) has been implicated as an important factor. PDA resulted in markedly increased WSS in the pulmonary arteries while leading to decreased WSS in the MBTS. Although in each case average WSS in the MBTS was below previously reported values for platelet activation (i.e. $< 315 \text{ dyn/cm}^2$) [20], WSS near anastomoses, was greater, suggesting possible platelet activation and thrombotic risk. The increase in RT within the MBTS for the case with PDA may increase the risk of shunt thrombosis by allowing for a greater opportunity for platelet deposition and aggregation following activation. Although flow through both the MBTS and PDA was mostly laminar ($Re < 2000$ for most cases; exceptions occurred for a few of the MBTS with PDA cases with the lowest PVR index values; $Re \sim 2200$), regions immediately preceding the proximal anastomoses and the pulmonary arteries following the distal anastomoses exhibited recirculation, the later appearing more pronounced. Consequently, platelet activation could lead to the expansion of thrombosis from the MBTS into the pulmonary arteries near the anastomosis. Furthermore, the thrombus formed could conceivably lyse (break off) leading to complication such as pulmonary embolism, heart attack, or stroke.

Although model predictions suggest a possible increase in thrombotic risk following PDA preservation, the association is not immediately clear. As previously explained, MBTS with PDA resulted in a non-optimized shunt configuration which lead to elevated cardiac output and pulmonary perfusion. Because the surrogates used for assessing thrombotic risk are all functions of blood flow, predicted WSS within the MBTS were naturally lower whereas RT was expectedly higher. From our results, we can infer that MBTS with PDA does not only lead to over-shunting but may also increase the risk of thrombosis within the MBTS. This suggests that the two leading causes of morbidity and mortality associated with MBTS insertion, shunt thrombosis and over-shunting, each involve a blood coagulation component, the former being more obvious than the latter.

4.3.3. PDA preservation vs ligation

Thrombosis represents the most likely cause of shunt occlusion. Although preserving the PDA allows for shunt redundancy, model predictions suggest that an MBTS with a PDA lead to pulmonary over-circulation and hypertension, while increasing the risk of thrombosis as flow through the MBTS decreases with respect to a configuration without a PDA. The main benefit of redundancy appears to be greater time for re-intervention in case of complications; but this must be weighed against

thrombotic risk.

PDA preservation, however, may be beneficial if establishing sufficient pulmonary circulation renders itself difficult. For example, in young neonates (< 2 wk) when PVR is naturally high, the PDA may be initially beneficial to help establish, together with the MBTS, sufficient pulmonary perfusion. In such situations, the PDA could initially act as a temporary “self-closing” shunt.

4.4. Other considerations and possible model extensions

As presented, our computational model applies for both univentricular and biventricular hearts, when there are no additional sources of blood flow to the pulmonary circulation other than the MBTS or MBTS plus PDA. This is because the heart was modeled as a pressure generator (using mean arterial pressure, MAP). Blood flow in our model adjusts to the patient MAP, reflecting the patient condition. Moreover, our model includes the geometry of the innominate, subclavian and pulmonary arteries (see Figure 1), and therefore variations in the size of these arteries, that occur in clinical practice, are taken into account. In clinical situations in which the subclavian artery is very small and flow limiting, or the arterial tree is anomalous, other arteries, such as the brachiocephalic artery are chosen as the inflow (proximal artery) for the shunt [21,22]. The computational model presented here could be easily extended to simulate the effect of various shunt sizes in situations in which the brachiocephalic artery, rather than the subclavian artery, is used as the shunt inflow.

The computational model described in this study considered a left aortic arch MBTS. In cases of complex cyanotic heart defects, however, aortic positions are variable, and sometimes the right aortic arch is used for the MBTS. Once again, our computational model could be easily extended for simulating a right aortic arch variant of the MBTS. This is indeed the case since the flow dynamics are similar in both cases and the only difference between these variants is the spatial configuration of the arch in relation to the pulmonary artery, which is taken into account by the modelled portion of the arterial branches (Figure 1). While we presented here a very specific example using the arterial geometry of one patient to model blood flow for that particular case, the model employed is versatile and can be adjusted to diverse anomalous geometries and patient situations.

5. Conclusions

The approach presented here could provide a step forward in intervention planning. Faster time to results (simulation time) can lead to testing of more scenarios, and to undergo sensitivity studies to fine-tune patient response parameters (e.g. LPN parameters) to more accurately model specific patients. The benefits of reduced computational expense in quickly estimating clinically relevant parameters (e.g. CI and Q_p/Q_s), enables a more thorough screen of surgical options, opening the doors for enhanced intervention planning through virtual surgery approaches. Patient specific CFD models could prove to be a useful clinical tool in the future by allowing for the preoperative simulation of a multitude of surgical scenarios and help inform clinicians as to the selection of the optimal approach.

Model predictions indicate that PDA ligation/preservation during MBTS insertion has a dramatic impact on postoperative circulation, the efficacy of which may be patient dependent. Our model also predicts that manipulating PVR is an effective means for reducing pulmonary arterial pressure in neonates with MBTS dependent circulations, without drastically altering overall

hemodynamics. Similar methodologies could be applied to a range of interventions beyond those intended to treat CCHD and could aid in the creation of new surgical strategies for cardiovascular disease.

Acknowledgments

The authors would like to thank Dr. Chivukula for advice during model implementation. This publication was made possible with support from the Oregon Clinical and Translational Research Institute (OCTRI), grant number UL1TR000128 from the National Center for Advancing Translational Sciences (NCATS), a component of the National Institutes of Health (NIH), and NIH Roadmap for Medical Research; and grant NIH R01 HL094570. The content is solely the responsibility of the authors and does not necessarily represent the official views of grant giving bodies.

Conflict of interest

The authors declare no conflicts of interest.

References

1. Petrucci O, O'Brien SM, Jacobs ML, et al. (2011) Risk factors for mortality and morbidity after the neonatal Blalock-Taussig shunt procedure. *Ann Thorac Surg* 92: 642–652.
2. Dirks V, Prêtre R, Knirsch W, et al. (2013) Modified Blalock Taussig shunt: a not-so-simple palliative procedure. *Eur J Cardio-Thorac Sur* 44: 1096–1102.
3. Li JS, Yow E, Berezny KY, et al. (2007) Clinical outcomes of palliative surgery including a systemic-to-pulmonary artery shunt in infants with cyanotic congenital heart disease: does aspirin make a difference?. *Circulation* 116: 293–297.
4. Pennati G, Corsini C, Hsia TY, et al. (2013) Computational fluid dynamics models and congenital heart diseases. *Front Pediatr* 1: 4.
5. Marsden AL, Feinstein JA (2015) Computational modeling and engineering in pediatric and congenital heart disease. *Curr Opin Pediatr* 27: 587.
6. Esmaily Moghadam M, Migliavacca F, Vignon-Clementel IE, et al. (2012) Optimization of shunt placement for the Norwood surgery using multi-domain modeling. *J Biomech Eng* 134: 051002.
7. Esmaily-Moghadam M, Murtuza B, Hsia TY, et al. (2015) Simulations reveal adverse hemodynamics in patients with multiple systemic to pulmonary shunts. *J Biomech Eng* 137: 031001.
8. Lagana K, Balossino R, Migliavacca F, et al. (2005) Multiscale modeling of the cardiovascular system: application to the study of pulmonary and coronary perfusions in the univentricular circulation. *J Biomech* 38: 1129–1141.
9. Hsia TY, Cosentino D, Corsini C, et al. (2011) Use of mathematical modeling to compare and predict hemodynamic effects between hybrid and surgical Norwood palliations for hypoplastic left heart syndrome. *Circulation* 124: S204–S210.
10. Arthurs CJ, Agarwal P, John AV, et al. (2017) Reproducing patient-specific hemodynamics in the Blalock–Taussig circulation using a flexible multi-domain simulation framework: applications

for optimal shunt design. *Front Pediatr* 5: 78.

11. Kowalski WJ, Teslovich NC, Dur O, et al. (2012) Computational hemodynamic optimization predicts dominant aortic arch selection is driven by embryonic outflow tract orientation in the chick embryo. *Biomech Model Mechan* 11: 1057–1073.
12. Migliavacca F, Pennati G, Dubini G, et al. (2001) Modeling of the Norwood circulation: effects of shunt size, vascular resistances, and heart rate. *Am J Physiol-Heart C Physiol* 280: H2076–H2086.
13. Piskin S, Altin HF, Yildiz O, et al. (2017) Hemodynamics of patient-specific aorta-pulmonary shunt configurations. *J Biomech* 50: 166–171.
14. Zahorec M, Hrubsova Z, Skrak P, et al. (2011) A comparison of Blalock-Taussig shunts with and without closure of the ductus arteriosus in neonates with pulmonary atresia. *Ann Thorac Surg* 92: 653–658.
15. Schiavazzi DE, Arbia G, Baker C, et al. (2016) Uncertainty quantification in virtual surgery hemodynamics predictions for single ventricle palliation. *Int J Numer Meth Bio Eng* 32: e02737.
16. Marsden AL, Feinstein JA, Taylor CA (2008) A computational framework for derivative-free optimization of cardiovascular geometries. *Comput Method Appl Mech Eng* 197: 1890–1905.
17. Winberg P, Lundell BP, Gustafsson LE (1994) Effect of inhaled nitric oxide on raised pulmonary vascular resistance in children with congenital heart disease. *Heart* 71: 282–286.
18. Nelson DP, Schwartz SM, Chang AC (2004) Neonatal physiology of the functionally univentricular heart. *Cardiol Young* 14: 52–60.
19. Turitto VT, Hall CL (1998) Mechanical factors affecting hemostasis and thrombosis. *Thromb Res* 92: S25–S31.
20. Holme PA, Ørvim U, Hamers MJAG, et al. (1997) Shear-induced platelet activation and platelet microparticle formation at blood flow conditions as in arteries with a severe stenosis. *Arterioscl, Throm, Vas Biol* 17: 646–653.
21. Chowdhury UK, Venugopal P, Kothari SS, et al. (2006) Criteria for selection of patients for, and results of, a new technique for construction of the modified Blalock-Taussig shunt. *Cardiol Young* 16: 463–473.
22. Chowdhury UK, George N, Sankhyan LK, et al. (2019) A novel surgical technique of construction of the modified Blalock-Taussig shunt (UKC's modification): A video presentation. *J Heart Cardiovas Med* 2: 025–026.



AIMS Press

© 2020 the Author(s), licensee AIMS Press. This is an open access article distributed under the terms of the Creative Commons Attribution License (<http://creativecommons.org/licenses/by/4.0>)